Journal of Biomedical Optics 5(2), 173–184 (April 2000)

Photon migration through fetal head *in utero* using continuous wave, near infrared spectroscopy: clinical and experimental model studies

Nirmala Ramanujam
Gargi Vishnoi
University of Pennsylvania
Dept. of Biochemistry and Biophysics
Philadelphia, Pennsylvania

Andreas Hielscher
State University of New York
Downstate Medical Center
Department of Pathology
Brooklyn, New York

Martha Rode
Iraj Forouzan
Hospital of the University of Pennsylvania
Dept. of Maternal–Fetal Medicine
Philadelphia, Pennsylvania

Britton Chance
University of Pennsylvania
Dept. of Biochemistry and Biophysics
Philadelphia, Pennsylvania

Abstract. Near infrared (NIR) measurements were made from the maternal abdomen (clinical studies) and laboratory tissue phantoms (experimental studies) to gain insight into photon migration through the fetal head *in utero*. Specifically, a continuous wave spectrometer was modified and employed to make NIR measurements at 760 and 850 nm, at a large (10 cm) and small (2.5/4 cm) source-detector separation, simultaneously, on the maternal abdomen, directly above the fetal head. A total of 19 patients were evaluated, whose average gestational age and fetal head depth, were 37 weeks ± 3 and 2.25 cm ± 0.7, respectively. At the large source-detector separation, the photons are expected to migrate through both the underlying maternal and fetal tissues before being detected at the surface, while at the short source-detector separation, the photons are expected to migrate primarily through the superficial maternal tissues before being detected. Second, similar NIR measurements were made on laboratory tissue phantoms, with variable optical properties and physical geometries. The variable optical properties were obtained using different concentrations of India ink and Intralipid in water, while the variable physical geometries were realized by employing glass containers of different shapes and sizes. Third, the NIR measurements, which were made on the laboratory tissue phantoms, were compared to the NIR measurements made on the maternal abdomen to determine which tissue phantom best simulates the photon migration path through the fetal head *in utero*. The results of the comparison were used to provide insight into the optical properties and physical geometry of the maternal and fetal tissues in the photon migration path. [S1083-3668(00)00702-4]

Keywords: near-infrared spectroscopy; photon migration; transabdominal; fetus; *in utero*; cerebral; blood oxygenation; laboratory tissue phantoms.

Paper JBO-42009 received Sep. 3, 1999; revised manuscript received Feb. 10, 2000; accepted for publication Feb. 28, 2000.

1 Introduction

Hypoxic-ischemic encephalopathy (HIE) and germinal-matrix intraventricular hemorrhage (IVH) are significant contributors to neuro-developmental abnormalities in fetuses.[1–3] In order to reduce the long-term morbidity associated with fetal neurological injury, the obstetrician must be concerned with the early detection of fetal neurological compromise *in utero* and timely delivery of such fetuses. Fetal heart rate monitoring, either alone as the nonstress test (NST) or as part of the biophysical profile (BPP), which includes serial ultrasonographic examination has been employed in the United States to provide an indirect measurement of fetal cerebral hemodynamics and oxygenation *in utero*. These ante-partum assessment tests, which are more frequently performed on high-risk populations, have reduced the frequency of fetal deaths.[4] However, these tests have also led in part to low birth weight, preterm delivery, cesarean delivery, and increased expense of care.[5] This is most likely due to the false-positive rate of the NST and BPP, which are 75%–90%[6] and 20%–75%,[7] respectively. As a result, the timely delivery of a neurologically compromised fetus is predicated by the fear of premature delivery of a neurologically healthy fetus, with a false-positive, ante-partum assessment test. This dilemma necessitates the need to reduce the false-positive rate of current ante-partum assessment tests for the detection of fetal neurological compromise *in utero*.

Noninvasive and fast, transabdominal, near infrared (NIR) spectroscopy of fetal cerebral blood oxygenation *in utero* may potentially avoid many of the pitfalls of current ante-partum assessment tests. Implementation of transabdominal, NIR spectroscopy involves several important requirements. First, the feasibility of performing NIR photon migration measurements through the fetal head *in utero* has to be demonstrated. Second, a quantitative NIR method that can selectively measure and quantify fetal cerebral blood oxygenation and vol-

Address all correspondence to Nirmala Ramanujam; E-mail: nimmi@mail.med.upenn.edu

1083-3668/2000/$15.00 © 2000 SPIE

ume *in utero* has to be developed and validated. Third, the efficacy of this technique has to be tested in a clinical setting.

In order to demonstrate feasibility, two key requirements have to be fulfilled. The first requirement is illumination of and detection from tissues at a minimum of two wavelengths, which lie within the absorption bands of oxygenated and deoxygenated hemoglobin between 700 and 900 nm.[8] The second requirement is placement of a source and detector pair on the maternal abdomen above the fetal head, at a large enough separation for light from the source to propagate through the maternal and fetal tissues, via a banana-shaped photon migration path, before being detected at the surface.[9] The customization of the well-established NIR technology[10] for this particular application, which has not been previously undertaken, could potentially represent a significant advance in perinatal care and NIR spectroscopy of large, deeply buried organs in the human body.

The feasibility of performing transabdominal, NIR spectroscopy on patients undergoing a routine NST has been reported previously.[11] Specifically, a continuous wave (cw) spectrometer was developed and employed to make NIR measurements at 760 and 850 nm, at a 10 cm source-detector separation on the maternal abdomen, directly above the fetal head. A total of 32 patients were evaluated, whose average gestational age and fetal head depth, were 37 weeks ± 3 and 2.3 cm ± 0.6, respectively. The NIR measurements were used to estimate relative changes in blood oxygenation and volume of the tissues being probed. Evaluation of the results indicates that: (1) NIR measurements can be made with an excellent signal to noise ratio from human tissues at a 10 cm source-detector separation, and (2) the blood oxygenation and volume changes, which were calculated from the NIR measurements suggest that the photon migration path at a 10 cm source-detector separation partially intercepts the underlying fetal head.

Subsequently in the current investigation, NIR measurements were made from the maternal abdomen (clinical studies) and laboratory tissue phantoms (experimental studies) to gain insight into photon migration through the fetal head *in utero*. Specifically, a (cw) spectrometer was modified and employed to make NIR measurements at 760 and 850 nm, not only at a large (10 cm), but also small (2.5/4 cm) source-detector separation, simultaneously, on the maternal abdomen, directly above the fetal head. A total of 19 patients were evaluated, whose average gestational age and fetal head depth, were 37 weeks ± 3 and 2.25 cm ± 0.7, respectively. At the large source-detector separation, the photons are expected to migrate through both the underlying maternal and fetal tissues before being detected at the surface, while at the short source-detector separation, the photons are expected to migrate primarily through the superficial maternal tissues before being detected. Second, similar NIR measurements were made on laboratory tissue phantoms, with variable optical properties and physical geometries. The variable optical properties were obtained using different concentrations of India ink and Intralipid in water, while the variable physical geometries were realized by employing glass containers of different shapes and sizes. Subsequently, the NIR measurements, which were made on the laboratory tissue phantoms, were compared to the NIR measurements made on the maternal abdomen to determine which tissue phantom best simulates the photon migration path through the fetal head *in utero*. The results of the comparison were used to provide insight into the optical properties and physical geometry of the maternal and fetal tissues in the photon migration path.

2 Materials and Methods

2.1 Instrumentation

Figures 1(a)–1(c) displays a schematic of (a) the cw, NIR spectrometer, (b) the corresponding optical probe, which contains two source-detector pairs, and (c) its placement on the maternal abdomen. The cw, NIR spectrometer incorporates a 12 V direct current (dc) power supply (MG Proseries, No. PS12), a frequency divider, three relays (Radio Shack, No. 9533), a halogen light source (Radio Shack, No. 272-1177) with dc brushless micro fans for cooling (Radio Shack, No. 273-240), a pair of tungsten light sources (Gilway Technical Lamps, No. 7152-A514), a pair of silicon photo detectors (Hamamatsu, No. S1337-66BR) filtered at 760 and 850 nm respectively, an analog differential processing circuit (NIM Incorporated, Runman™), and a computer with a 12 bit analogue-to-digital (A/D) board.

The Runman™ power supply produces a 5 V, output pulse at a frequency of 0.5 Hz (1). The frequency divider splits this into output pulses (2) and (3), which are at a frequency of 0.0625 Hz and out of phase by 180°. Output pulse (2) combines with (1) (generated by the Runman™ power supply) in a relay to produce output pulse (5). Output pulse (3) combines with (1) (generated by the Runman™ power supply) in a relay to produce output pulse (4). Output pulse (4) combines with (7) (from the dc line of a 12 V power supply) in a relay to produce output pulse (6). Output pulses, (5) and (6) are identical except for being out of phase by 180° and having different peak voltages. Output pulses (5) and (6) control the tungsten and the halogen light sources, respectively at a time sharing frequency of 0.0625 Hz. Furthermore, each light source is modulated at a frequency of 0.5 Hz in order to minimize the interference of ambient light.

The halogen and tungsten light sources and the pair of silicon photo detectors are fixed securely in a flexible rubber pad. The halogen light source consists of four, 20 W halogen light bulbs filtered using a 700-nm-long pass filter. Cooling fans on either side of the lamp housing are employed to reduce the effect of the heat generated by the halogen bulbs. The halogen light source is placed at a 10 cm separation from the pair of silicon photodetectors (to achieve a penetration depth of ~ 3 cm in tissue). The pair of 0.575 W tungsten light sources is placed at either a 4 or 2.5 cm separation on either side of the pair of silicon photodetectors (to achieve a penetration depth of $\sim 1-2$ cm in the tissue).

The pair of silicon photo detectors receives the time-shared, optical inputs from the tissue (which is illuminated alternately by the halogen and tungsten light sources) that are filtered at 760 and 850 nm by ± 10 nm band pass filters. The resulting electronic outputs at the two wavelengths are differentially amplified using the Runman™ to provide their difference and sum at the two source-detector separations. Two potentiometers in the Runman™ circuit can be used to adjust the balance and gain of the outputs. The balance adjustment allows for the outputs at 760 and 850 nm measured from the tissue to be equilibrated such that the difference is zero. In

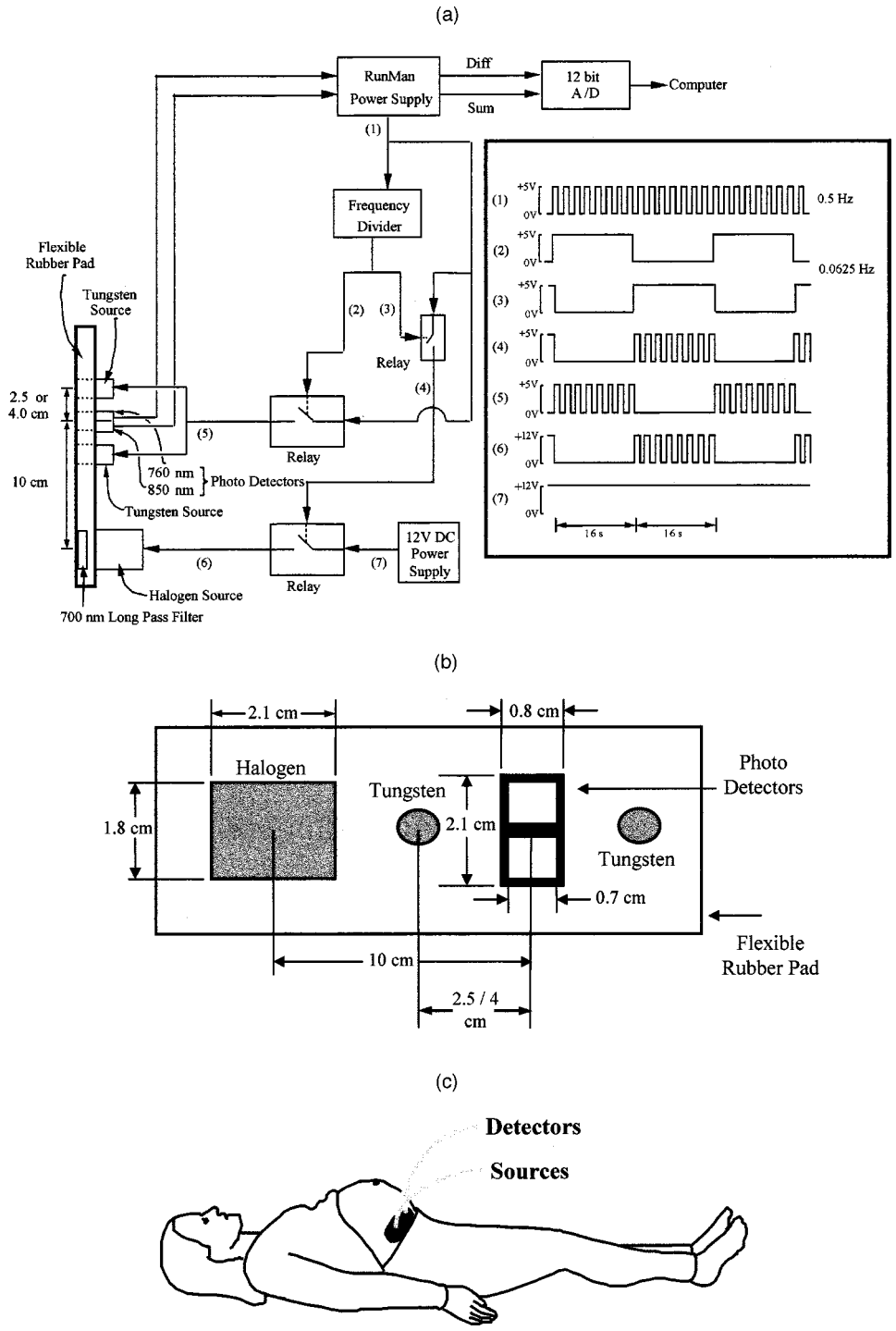

Fig. 1 A schematic of (a) the cw, NIR spectrometer, (b) the corresponding optical probe, which contains two source-detector pairs, and (c) its placement on the maternal abdomen.

adjusting the outputs at 760 and 850 nm to equality, their relative sensitivity is altered. The gain adjustment allows for the amplification of the outputs at 760 and 850 nm. A toggle switch with three settings can be used to choose one of three possible outputs: (1) the difference and sum of the outputs at 760 and 850 nm, (2) the output at 760 nm, or (3) the output at 850 nm. The output is digitized using a 12-bit A/D board, integrated for 2 s and then stored on a personal computer.

2.2 Transabdominal, NIR Measurements

Transabdominal measurements were performed on a total of 19 patients undergoing a routine NST in which fetal heart rate and uterine contractions were simultaneously monitored for approximately 20–40 min to assess fetal well being. The average age of the patients was 28 years ± 6 and their average gestational age was 37 weeks ± 3. This study was reviewed

and approved by the Institutional Review Boards of the University of Pennsylvania and written consent was obtained from all patients that participated. Two types of transabdominal, NIR measurements were made. First, a continuous NIR measurement was made on the mid line of the maternal abdomen during the NST period. After the NST, NIR measurements were made as a function of three different lateral positions of the optical probe on the maternal abdomen.

Details of the clinical protocol are described elsewhere.[11] Briefly, an ultrasound exam was performed to determine the position of the fetal head and the placenta within the uterus and the distance between the ultrasound transducer and the fetal head. The average distance between the fetal brain and the ultrasound transducer was 2.25 cm $\pm$ 0.7. A Doppler transducer and a pressure-sensitive tocodynamometer were attached to the maternal abdomen to monitor the fetal heart rate and uterine contractions, respectively, as part of the NST.

The optical probe was then placed on the maternal abdomen right above the pubic bone, such that the large source-detector pair straddled the mid line, under which the fetal head was generally located [Figure 1(c)]. The cw spectrometer was equilibrated using the balance potentiometer to set the base line outputs to be equivalent at 760 and 850 nm. Equilibration was performed when the fetal heart rate was stable and in the absence of uterine contractions. The NIR measurement was commenced and synchronized in time with the fetal heart rate and uterine contraction measurements. The continuous NIR measurement was performed for the duration of the NST period. After the NST, NIR measurements were made as a function of three different lateral positions of the optical probe on the maternal abdomen. In the first position, the large source-detector pair was straddled on the mid line (under which the fetal head was located). The two other positions were achieved by shifting this pair to the lateral left and right of the mid line, such that the fetal head was either directly below the source or directly below the detector. Next, the optical probe was placed in contact with a solid resin, calibration model made up of Titanium Dioxide (Sigma) and Ink (Pelican, Fount India) (absorption and reduced scattering coefficient of 0.15 and 5 cm^{-1}, respectively at 750 and 850 nm). The NIR measurements from the maternal abdomen were divided by the NIR measurements from the calibration model, in order to correct for variations in the source intensity and throughput of the device.

Measurements were made on the mid line of the abdomen of 10 patients at a 10 and 4 cm source-detector separation and on the mid line of the abdomen of 9 patients at a 10 and 2.5 cm source-detector separation. Measurements were made as a function of three different positions of the optical probe on the maternal abdomen of 13 patients.

2.3 NIR Measurements on Laboratory Tissue Phantoms

NIR measurements were made from two types of laboratory tissue phantoms to determine which best simulates the measurements made from the maternal abdomen. Figures 2(a) and 2(b) display a schematic of the two tissue phantoms, which consist of three glass containers representing the maternal tissue layer, which comprises the abdominal and uterine tissues (C), the amniotic fluid sac in the uterus (B), and the fetal head

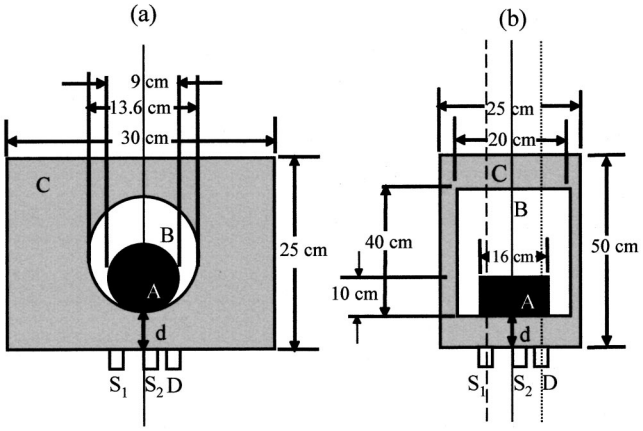

Fig. 2 A schematic of the two tissue phantoms, which consist of three glass containers representing the maternal tissue layer (C), the amniotic fluid sac (B), and the fetal head (A). In (a), containers B and A are cylindrical, while in (b), containers B and A are rectangular. In each tissue phantom, the absorption and scattering coefficients of containers C and A were set using solutions of India Ink and Intralipid in water, while that of container B was set using distilled water. The absorption and reduced scattering coefficients were 0.15 and 5 cm^{-1}, respectively, for container A. The absorption coefficient of container C was varied from 0.02 to 0.1 cm^{-1} in 0.02 cm^{-1} increments for a constant reduced scattering coefficient of 5 cm^{-1}. The fetal head depth is defined by d. $S_1 - D$ represents a 10 cm source-detector separation and $S_2 - D$ represents a 2.5 cm source-detector separation. The solid line represents the mid line of $S_1 - D$ (mid line position), the dashed line represents the mid line of S_1 (source position), and the dotted line represents the mid line of D (detector position).

(A). In Fig. 2(a), containers B and A are cylindrical, resulting in nonuniform contact between them, while in Fig. 2(b), containers B and A are rectangular, resulting in uniform contact between these two containers. In each tissue phantom, the absorption and reduced scattering coefficients of containers C and A were set using solutions of India Ink (Pelican, Fount India) and Intralipid (Pharmacia and Upjohn Company, Intralipid 30%) in water, while that of container B was set using distilled water. The absorption and reduced scattering coefficients were independently quantified from fits of the time resolved reflectance measurement of the solutions in containers C and A to the time-dependent diffusion equation for a semi-infinite geometry.[12,13] The absorption and reduced scattering coefficients were 0.15 and 5 cm^{-1}, respectively for container A. The absorption coefficient of container C was varied from 0.02 to 0.1 cm^{-1} in 0.02 cm^{-1} increments for a constant reduced scattering coefficient of 5 cm^{-1}. The absorption and reduced scattering coefficients for containers C and A were selected such that they are within the range reported in the literature for muscle and fat (for the maternal tissue) and the neonatal head (for the fetal tissue), respectively.[14]

In Figures 2(a) and 2(b), the fetal head depth or synonymously, the maternal tissue thickness is defined by ''d.'' ''$S_1 - D$'' corresponds to a 10 cm source-detector separation and ''$S_2 - D$'' corresponds to a 2.5 cm source-detector separation. In both tissue phantoms, the optical probe was fixed on one of the walls of the outermost container C, such that the mid line between $S_1 - D$ coincides with the solid line, which

represents the mid line of that wall. Furthermore, in each tissue phantom, containers B and A were also centered on the solid line. Finally, in each tissue phantom, container A was placed in contact with container B such that the distance, d between the inner wall of container C and the outer walls of containers B and A were equivalent (assuming that the wall thickness of containers A and B are negligible compared to d). These physical geometries were intended to simulate a late gestational fetal head *in utero*, which is in contact with the maternal tissue, as was observed by ultrasonographic examination in the clinical setting.

In the first experiment, measurements at the 10 and 2.5 cm source-detector separations were made as a function of d, which was varied, from 1 to 4 cm, in 1 cm increments. This experiment was performed for five different absorption coefficients in container C: 0.02, 0.04, 0.06, 0.08, and 0.1 cm^{-1}. This experiment was intended to simulate the NIR measurement made on the mid line of the maternal abdomen, after the NST. In the second experiment, NIR measurements at the 10 and 2.5 cm source-detector separations were made as a function of d (for a fixed absorption coefficient of 0.08 cm^{-1} in container C), for three different positions of container A, relative to the optical probe. This experiment was performed using only the tissue phantom shown in Figure 2(b). The first position was achieved by positioning container A such that it was centered on the solid line, which represents the mid line of S_1-D on the wall of container C (mid line position). The second position was achieved by positioning container A such that it was centered on the dashed line that represents the mid line of ''S_1'' on the wall of container C (source position). The third position was achieved by positioning container A such that it was centered on the dotted line, which represents the mid line of ''D'' on the wall of container C (detector position). This experiment was intended to simulate the NIR measurement made as a function of three different positions of the optical probe on the maternal abdomen, after the NST. However, note that container A (which represents the fetal head), rather than the optical probe was displaced to achieve the three different positions of the optical probe on the maternal abdomen.

2.4 Data Analysis

The absorption (A) at each wavelength was calculated according to Eq. (1), which is based on the Beer–Lambert Law[15]

$$A = \log_{10}\left(\frac{I_o}{I}\right), \tag{1}$$

where, I_o is the base line intensity at each wavelength and I is the intensity at each wavelength during the NIR measurement period.

The relative changes in blood oxygenation and volume were calculated from the NIR measurements made at 760 and 850 nm using the following empirically derived equations.[11] These equations were obtained from NIR measurements of blood containing tissue phantoms.

$$\Delta\text{o.d.} = \log\left(\frac{I_o}{I_{850\text{ nm}}}\right) - \log\left(\frac{I_o}{I_{760\text{ nm}}}\right) \tag{2a}$$

$$\Sigma\text{o.d.} = 0.01\times\log\left(\frac{I_o}{I_{760\text{ nm}}}\right) + 0.27\times\log\left(\frac{I_o}{I_{850\text{ nm}}}\right). \tag{2b}$$

Here, Δo.d. is the blood oxygenation index, and Σo.d. is the blood volume index, $I_{760\text{ nm}}$ and $I_{850\text{ nm}}$ are the re-emitted intensities at 760 and 850 nm, respectively, and I_o is the baseline intensity at each wavelength. The baseline intensity, I_o was defined specifically for each measurement. The coefficients were selected for Eqs. (2a) and (2b) such that there is minimal cross-talk between blood oxygenation and blood volume indices. The coefficients selected are device specific and therefore are not only related to the absorption characteristics of hemoglobin at the specific wavelengths but also the source strength and detector response of the instrument.

3 Results and Discussion

3.1 Transabdominal, NIR Measurements

Figures 3(a) and 3(b) displays typical blood oxygenation and volume indices, calculated from NIR measurements at a 10 cm and a 4/2.5 cm source-detector separation on the mid line of the abdomen of two patients during the NST period. Corresponding fetal heart rate and uterine contraction traces are also shown. In both patients, NIR measurements were made over a period of approximately 20 min. First, the absorption was calculated from the NIR measurements at each wavelength. The blood oxygenation and volume indices were calculated from NIR intensities measured at 760 and 850 nm using Eqs. (2a) and (2b), respectively, and postprocessed with a three point moving average. In both patients, there are several spontaneous accelerations in the heart rate (an increase in the fetal heart rate by at least 15 beats per minute for 15 s) and uterine contractions are absent. In Figure 3(a), the fetal gestational age is 35 weeks and the fetal head depth is 13 mm, while in Figure 3(b), the fetal gestational age is 40 weeks and the fetal head depth is 29 mm. Evaluation of Figures 3(a) and 3(b), indicates that NIR measurements from the maternal abdomen can be obtained with a good signal-to-noise ratio (which is approximately 50:1 in these traces) at both the large and small source-detector separations.

Figures 4(a) and 4(b) displays the mean and standard deviation of (a) the blood oxygenation index and (b) the blood volume index at the 10 and 4/2.5 cm source-detector separations on the mid line of the maternal abdomen during the NST period. Figure 4(a) shows that the mean and standard deviation of blood oxygenation index at the 10 cm source-detector separation, is on average significantly greater than that at the 4/2.5 cm source-detector separation from the same patient. Evaluation of Figure 4(b) indicates that the mean of blood volume index at the 10 and 4/2.5 cm source-detector separations from the same patient are relatively more comparable. However, the standard deviation of the blood volume index is significantly greater at the 10 cm source-detector separation, relative to that at the 4/2.5 cm source-detector separation. These results clearly indicate that there are significant differences in the blood oxygenation and blood volume indices at the large and small source-detector separations. Hence, the use of several (large and small) source-detector separations can be used to discern between a combination of maternal and fetal responses from a maternal-only response.

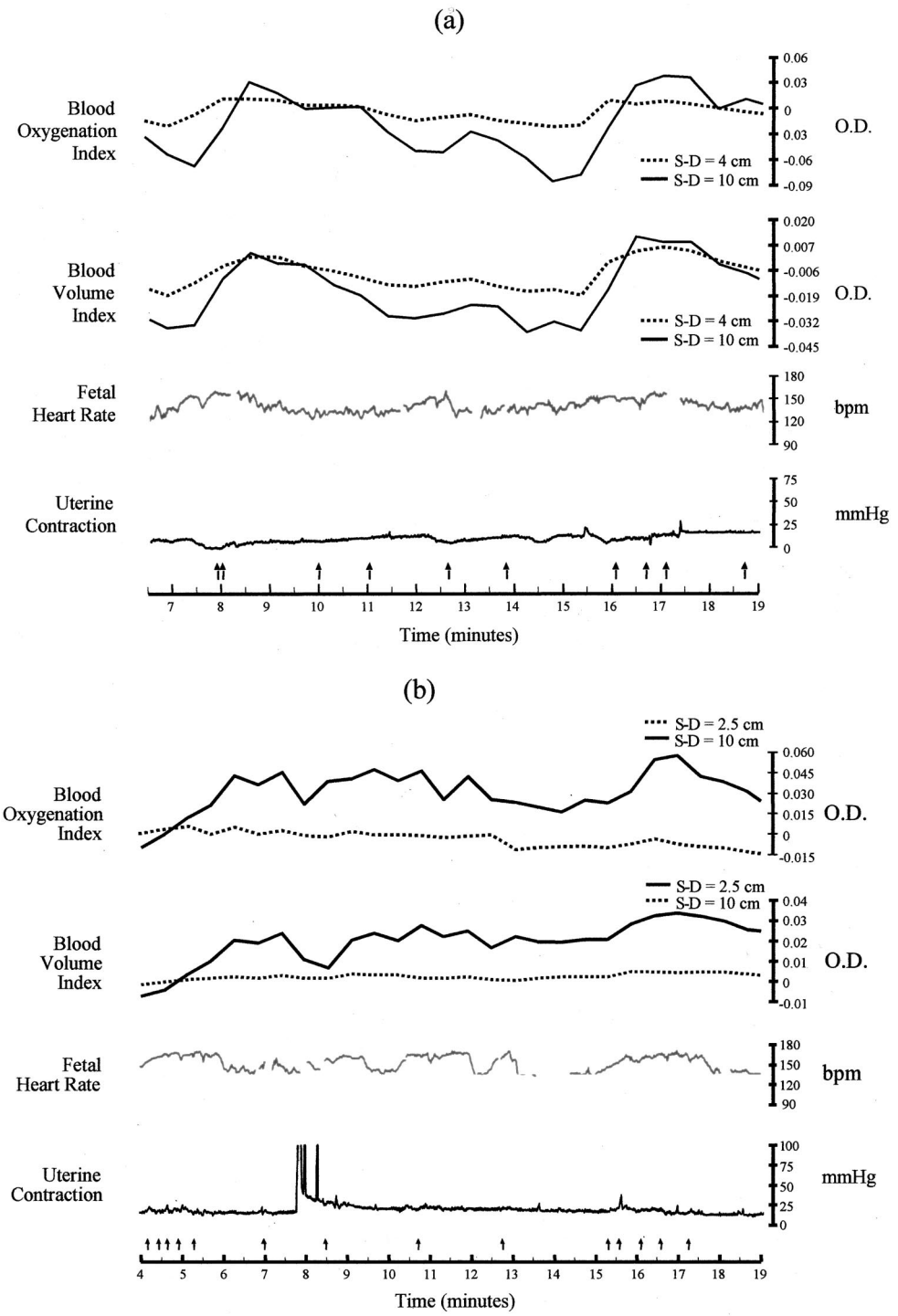

Fig. 3 Blood oxygenation and volume indices [optical density (o.d.)], quantified from NIR measurements made at a 10 and a 4/2.5 cm source-detector separation on the mid line of the abdomen of two patients, during the NST period and corresponding fetal heart rate [beats per minute (bpm)] and uterine contraction [millimeters of mercury (mm Hg)] traces. The blood oxygenation and volume indices were calculated from NIR intensities measured at 760 and 850 nm using Eqs. (2a) and (2b), respectively, and postprocessed with a three point moving average to improve the signal-to-noise ratio, which is approximately 50:1 in these traces. In both patients, there are several spontaneous accelerations in the heart rate (an increase in the fetal heart rate by at least 15 bpm for 15 s) and uterine contractions are absent. In (a), the fetal gestational age is 35 weeks and the fetal head depth is 13 mm, while in (b), the fetal gestational age is 40 weeks and the fetal head depth is 29 mm.

In Figures 3(a), 3(b), 4(a), and 4(b) it is difficult to rule out the potential contribution of fetal motion artifacts [see arrows at the bottom of Figures 3(a) and 3(b) which indicate maternal perception of fetal movement] to the blood oxygenation and volume indices, calculated from the NIR measurements made at the 4/2.5 cm source-detector separation and particularly, those at the 10 cm source-detector separation. To provide insight into this potential problem, the hypothesis that an in-

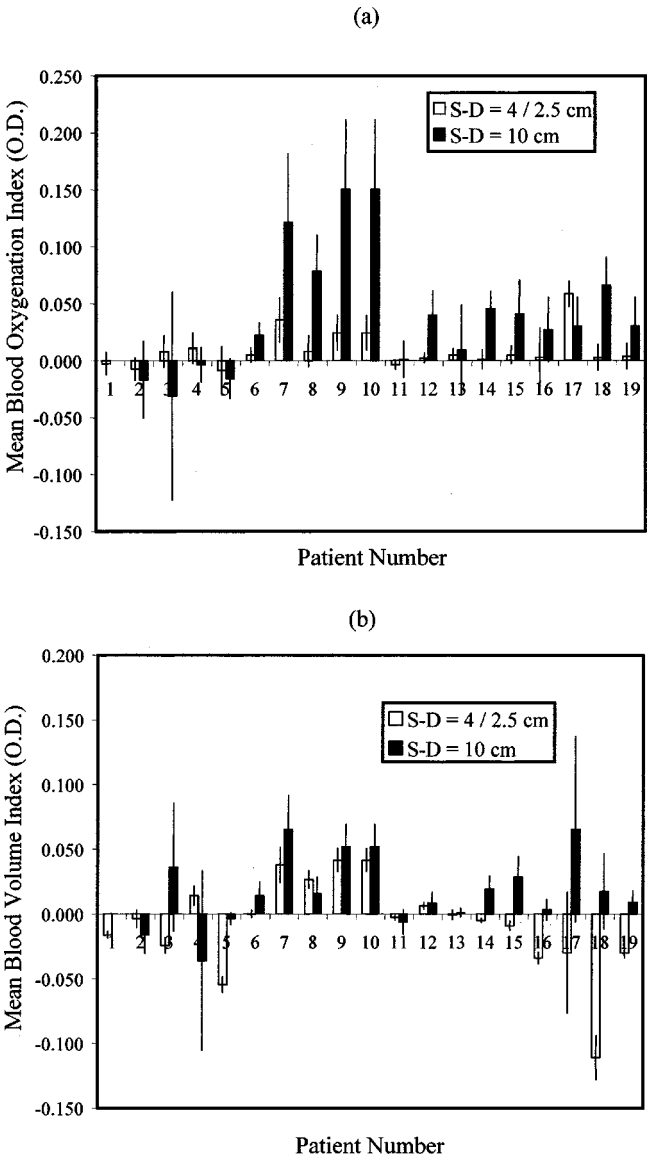

Fig. 4 Mean and standard deviation of (a) the blood oxygenation index and (b) the blood volume index, quantified from NIR measurements made at both the 10 and 4/2.5 cm source-detector separations on the mid line of the maternal abdomen, during the NST period.

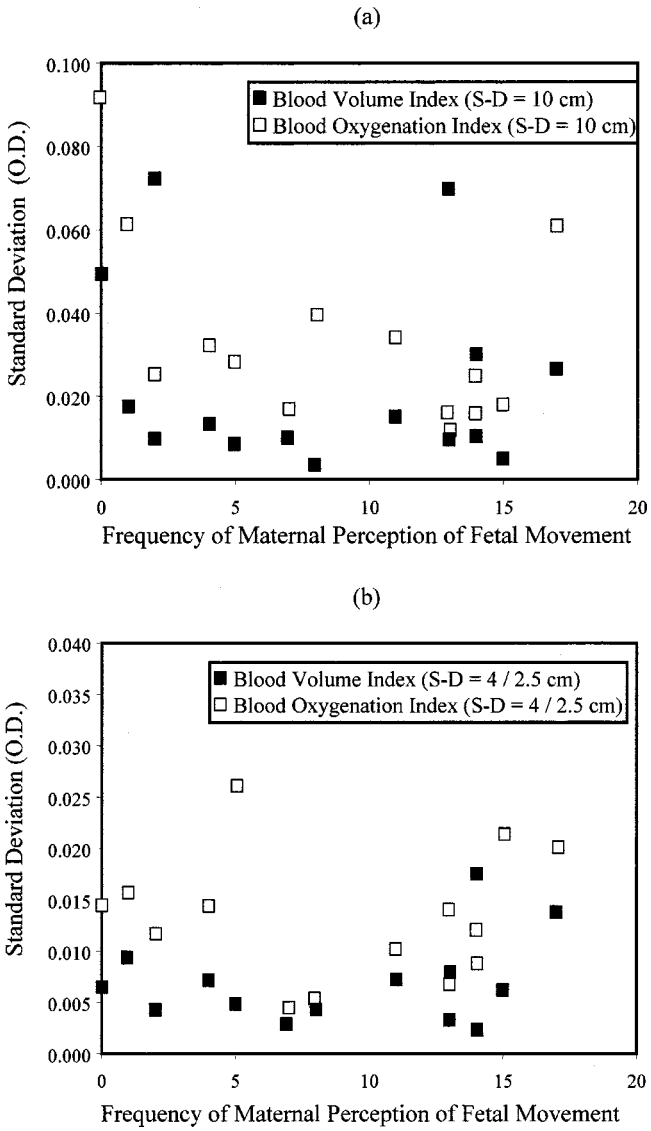

Fig. 5 The correlation between the frequency of maternal perception of fetal movement and the standard deviation in the blood oxygenation and volume indices, calculated from the NIR measurements made on the mid line of the maternal abdomen during the NST period at (a) the 10 and (b) the 4/2.5 cm source-detector separation.

crease in the frequency of fetal movement should cause an increase in the variation of the blood oxygenation and volume indices during the NST period was tested. Specifically, the relationship between the standard deviation in the blood oxygenation and volume indices and the frequency of maternal perception of fetal movement was evaluated. For each patient, the standard deviation was calculated from the blood oxygenation and volume indices, obtained from the NIR measurements made at the 10 and 4/2.5 cm source-detector separations on the mid line of the maternal abdomen during the NST period. The frequency of maternal perception of fetal movement was determined by summing the number of electronically marked arrows in the fetal heart rate tracing during the NST period.

Figures 5(a) and 5(b) displays the correlation between the frequency of maternal perception of fetal movement and the standard deviation in the blood oxygenation and volume indices, calculated from the NIR measurements made on the mid line of the maternal abdomen during the NST period at (a) the 10 cm source-detector separation and (b) the 4/2.5 cm source-detector separation. Figures 5(a) and 5(b) indicates that the correlation coefficient between the frequency of maternal perception of fetal movement and the standard deviation in the blood oxygenation and volume indices at both the 10 and 4/2.5 cm source-detector separations is less than 0.01. Although these results are encouraging, more rigorous approaches, particularly unbiased, ultrasonographic examination of fetal movement will be incorporated into subsequent clinical investigations.

Figures 6(a) and 6(b) display the intensity at 760 nm in calibrated units (c.u.) as a function of fetal head depth, measured from the mid line of the maternal abdomen at (a) the 10

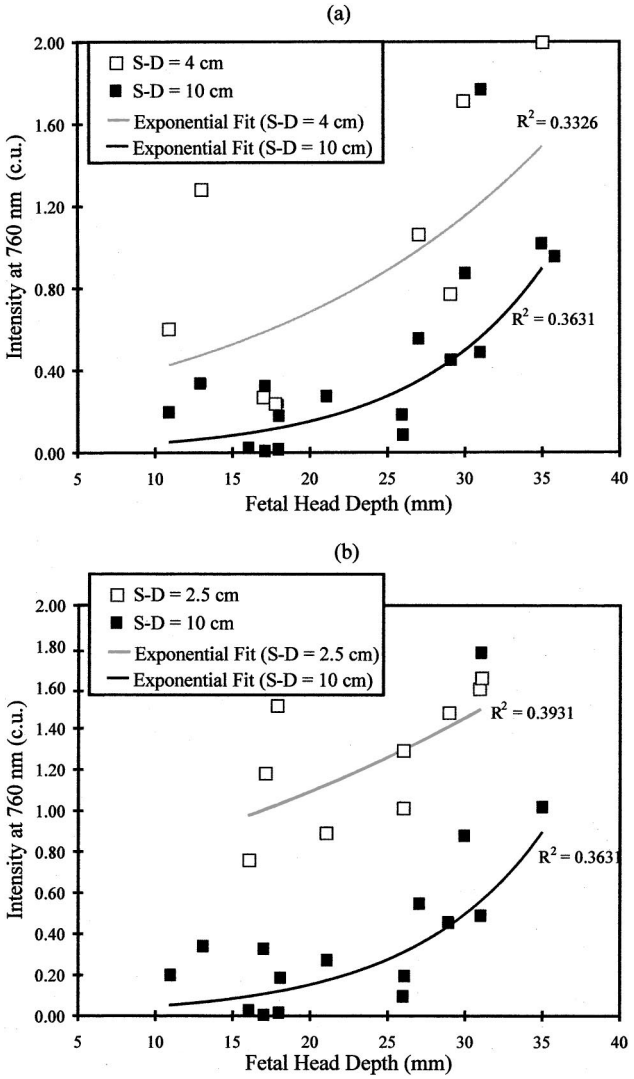

Fig. 6 Intensity at 760 nm in calibrated units (c.u.) as a function of fetal head depth, measured from the mid line of the maternal abdomen at the (a) 10 and 4 cm source-detector separations and (b) the 10 and 2.5 cm source-detector separations, after the NST. The solid lines represent a least squares fit of the intensity-depth profile at each source-detector separation to an exponential function. The term, R^2, which represents the goodness of fit, is defined as one less the ratio of the sum of the square of the errors (SSE) and the sum of the square of the total (SST). An increase in R^2 reflects an increase in the goodness of the fit.

and 4 cm source-detector separations and (b) the 10 and 2.5 cm source-detector separations, after the NST. The calibration of the intensity refers to the correction of the measured intensity for variations in the source intensity and throughput of the device, which has been achieved by normalizing it to the intensity measured from a solid resin calibration model. The solid lines represent a least squares fit of the intensity-depth profile at each source-detector separation to an exponential function. The term, R^2, which represents the goodness of fit, is defined as one less the ratio of the sum of the square of the errors (SSE) and the sum of the square of the total (SST). An increase in R^2 reflects an increase in the goodness of the fit.

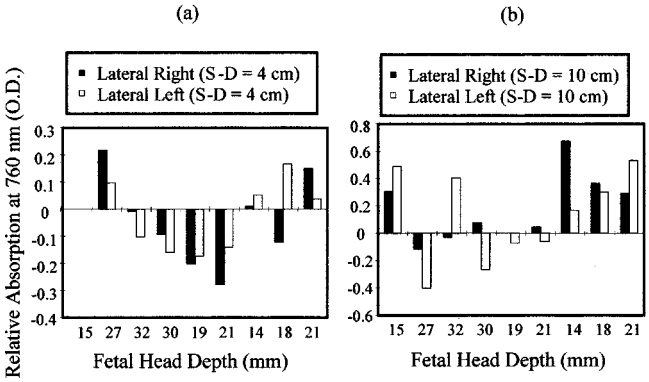

Fig. 7 The absorption at 760 nm measured from the lateral left and lateral right of the mid line of the maternal abdomen at (a) a 4 and (b) a 10 cm source-detector separation, after the NST. The absorption was calculated using Eq. (1); the intensity measured at the lateral left, lateral right, and the mid line were normalized to that at the mid line (such that the absorption is zero at the mid line of the maternal abdomen). Fetal head depths in these measurements ranged from 14 to 32 mm.

Evaluation of Figures 6(a) and 6(b) indicates that the intensity at 760 nm measured at the 10 cm source-detector separation is relatively invariant for fetal head depths of up to 20 mm; above 20 mm, there is a significant increase in the intensity. The exponential increase in intensity with increasing fetal head depth clearly suggests that the fetal head partially intercepts the photon migration path and that it is a more absorbing medium than the maternal tissue. Evaluation of Figure 6(a) indicates that the intensity measured at the 4 cm source-detector separation increases exponentially with increasing fetal head depth as was observed at the 10 cm source-detector separation, while evaluation of Figure 6(b) indicates that the intensity measured at the 2.5 cm source-detector separation increases linearly rather than exponentially with increasing fetal head depth. A similar phenomenon is observed for all three source-detector separations at 850 nm.

Figures 7(a) and 7(b) displays the absorption at 760 nm measured from the lateral left and lateral right of the mid line of the maternal abdomen at (a) a 4 cm source-detector separation and (b) a 10 cm source-detector separation, after the NST. The absorption was calculated using Eq. (1); the intensity measured at the lateral left, lateral right, and the mid line were normalized to that at the mid line (such that the absorption is zero at the mid line of the maternal abdomen). Fetal head depths in these measurements ranged from 14 to 32 mm. Figure 7(a) shows that at the 4 cm source-detector separation, the absorption at both the lateral left and right are displaced in the same direction relative to that at the mid line except for the patient with a fetal head depth of 18 mm. In 50% of the patients, the absorption measured at the lateral left and right is less than that at the mid line. However, evaluation of Figure 7(b) indicates that at the 10 cm source-detector separation, the absorption at the lateral left and right are displaced in opposite directions relative to that at the mid line in 50% of the patients; at one lateral displacement, the absorption is increased relative to that at the mid line, while at the other it is decreased relative to that at the mid line. In the remaining 50%,

the absorption at both the lateral left and right is increased relative to that at the mid line. Note that a decrease in absorption at both the lateral left and right positions relative to that at the mid line is observed only for one patient with a fetal head depth of 27 mm.

3.2 NIR Measurements From Laboratory Tissue Phantoms

In order to simulate the clinical results shown in Figures 6(a) and 6(b), NIR measurements were made on the mid line of the tissue phantoms shown in Figures 2(a) and 2(b) at the 10 and 2.5 cm source-detector separations. NIR measurements were made as a function of d, which was varied from 1 to 4 cm, in 1 cm increments. This experiment was intended to simulate the NIR measurement made on the mid line of the maternal abdomen, after the NST.

Figures 8(a) and 8(b) display (a) the absorption at 760 nm, calculated from NIR measurements made at the 10 cm source-detector separation and (b) the ratio of the 760 nm intensities at the 10 and 2.5 cm source-detector separations, displayed as a function of fetal head depth, for the maternal abdomen and the tissue phantom [Figure 2(a)], which has nonuniform contact between the maternal tissue and fetal head. The absorption was calculated according to Eq. (1) by normalizing the intensity measured at each fetal head depth to that measured at the shortest fetal head depth. Evaluation of Figures 8(a) and 8(b) indicates that the absorption increases, while the ratio of intensities at the large and small source-detector separations decreases as a function of fetal head depth for the tissue phantom; this is the opposite of what is observed for the maternal abdomen. Furthermore, at a given fetal head depth, the absorption increases with an increased absorption coefficient in container C, which represents the maternal tissue layer.

Figures 9(a) and 9(b) displays (a) the absorption at 760 nm, calculated from NIR measurements at the 10 cm source-detector separation and (b) the ratio of the 760 nm intensities at the 10 and 4/2.5 cm source-detector separations, displayed as a function of fetal head depth for the maternal abdomen and the tissue phantom [Figure 2(b)], which has uniform contact between the maternal tissue and the fetal head. In this case, the absorption decreases, while the ratio of the intensities at the large and small source-detector separations, increases as a function of fetal head depth for both the tissue phantom and the maternal abdomen. Again, at a given fetal head depth, the absorption increases with an increased absorption coefficient in container C, which represents the maternal tissue layer.

Finally, a comparison between the results from the two tissue phantoms indicates that the absorption increases as a function of fetal head depth, when the amniotic fluid sac and the fetal head are simulated by cylindrical containers [Figure 8(a)], whereas the absorption decreases as a function of fetal head depth when the amniotic fluid sac and the fetal head are simulated by rectangular containers [Figure 9(a)]. The latter result should be expected here since the fetal head, which is relatively more absorbing than the maternal tissue contributes progressively less to the photon migration path, with increasing fetal head depth.

The paradoxical result observed in Figure 8(a) may be explained by numerical, finite-difference simulations that provide solutions to the diffusion and transport equations.[16] Briefly, when there is nonuniform contact between the maternal tissue and fetal head [Figure 2(a)], there will be intervening amniotic fluid between these two tissue layers. The amniotic fluid will divert a large fraction of the photons around the fetal head, before they are detected at the surface. It is expected that as the fetal head depth increases, the amniotic fluid and fetal head will contribute progressively less to the photon migration path, while the maternal tissue will contribute more to the photon migration path. This will result in an increase in the absorption with an increase in the fetal head depth as is observed in Figure 8(a). However, when there is uniform contact between the maternal tissue and fetal head [Figure 2(b)], there is minimal or no intervening amniotic fluid between these two tissue layers. In this case, a large fraction of the photons migrate through the fetal head, before they are detected at the surface. It is expected that as the fetal head depth increases, the fetal head will contribute progressively less to the photon migration path, but the less absorbing maternal tissue will contribute progressively more to the pho-

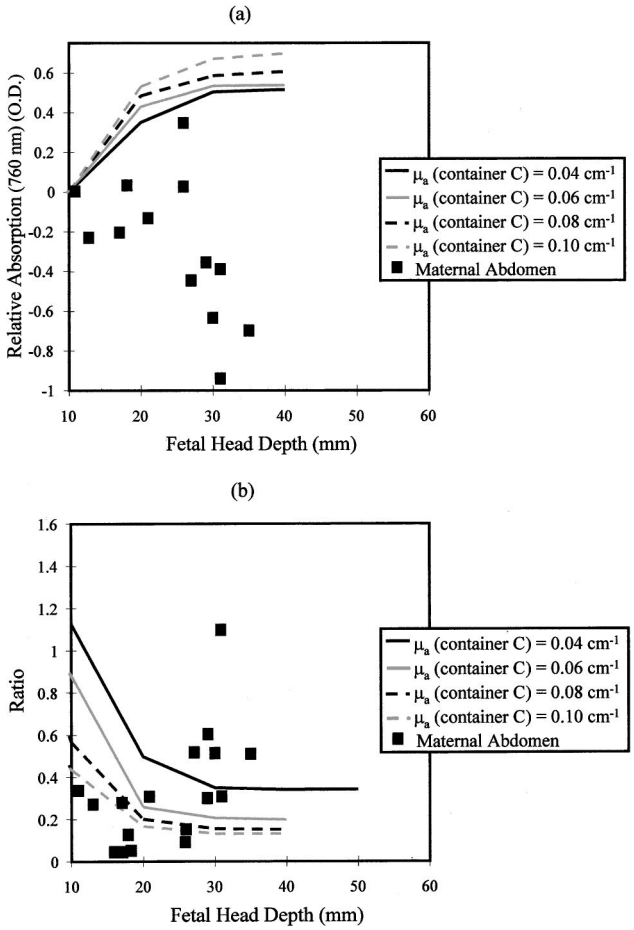

Fig. 8 (a) Absorption at 760 nm, calculated from NIR measurements made at the 10 cm source-detector separation and (b) ratio of 760 nm intensities at the 10 and 2.5 cm source-detector separations, displayed as a function of fetal head depth, for the maternal abdomen and the tissue phantom [Figure 2(a)], which has nonuniform contact between the maternal tissue and fetal head. Absorption was calculated according to Eq. (1) by normalizing the intensity measured at each fetal head depth to that measured at the shortest fetal head depth.

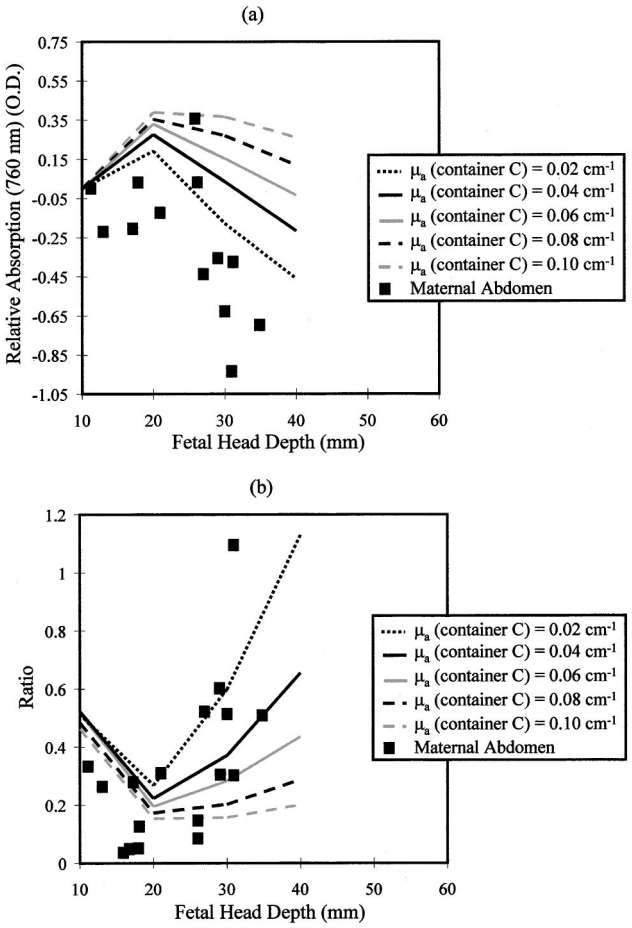

Fig. 9 (a) Absorption at 760 nm, calculated from NIR measurements at the 10 cm source-detector separation and (b) ratio of the 760 nm intensities at the 10 and 2.5 cm source-detector separations, displayed as a function of fetal head depth, for the maternal abdomen and the tissue phantom [Figure 2(b)], which has uniform contact between the maternal tissue and fetal head. Absorption was calculated according to Eq. (1) by normalizing the intensity measured at each fetal head depth to that measured at the shortest fetal head depth.

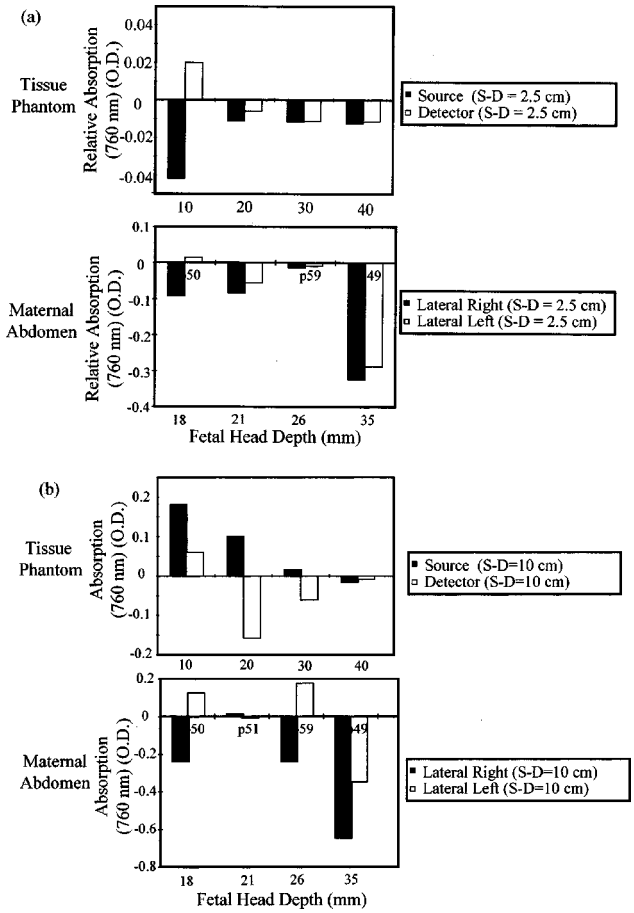

Fig. 10 Absorption at 760 nm, calculated from NIR measurements made at (a) a 2.5 and (b) a 10 cm source-detector separation from the tissue phantom shown in Figure 2(b) and from the maternal abdomen. NIR measurements on the tissue phantom were made as a function of three different positions of container A (which represents the fetal head), relative to the optical probe, whereas NIR measurements on the maternal abdomen were made as a function of three different positions of the optical probe, relative to the fetal head.

ton migration path. This will result in a decrease in the absorption as a function of fetal head depth as is observed in Figure 9(a). Evaluation of Figures 8(a) and 9(a) indicates that although the tissue phantom shown in Figure 2(a) simulates the anatomy of the fetal head *in utero*, the tissue phantom shown in Figure 2(b) simulates the photon migration path through the fetal head *in utero*. The tissue phantom shown in Figure 2(b) has two important characteristics. First, the fetal head is more absorbing than the maternal tissue layer. Second, there appears to be minimal intervening amniotic fluid between the maternal tissue and fetal head in the photon migration path, in the case of the late gestational fetal head *in utero*.

In order to simulate the clinical results shown in Figures 7(a) and 7(b), NIR measurements were made on the tissue phantom shown in Figure 2(b) at the 2.5 and 10 cm source-detector separations. NIR measurements were made as a function of d for three different positions of container A (mid line, source, and detector positions), relative to the optical probe. This experiment was intended to simulate the NIR measurements made as a function of three different positions of the optical probe on the maternal abdomen, after the NST. However, note that container A (which represents the fetal head) rather than the optical probe was displaced to achieve the three different positions of the optical probe on the maternal abdomen.

Figures 10(a) and 10(b) displays the absorption at 760 nm, calculated from NIR measurements at (a) a 2.5 cm source-detector separation and (b) a 10 cm source-detector separation from the tissue phantom shown in Figure 2(b) and from the maternal abdomen. Evaluation of the NIR measurements from the tissue phantom in Figure 10(a) indicates that at a source-detector separation of 2.5 cm and at a fetal head depth of 10 mm, the absorption is increased relative to that at the mid line when the fetal head is directly below the detector and decreased relative to the mid line when it is directly below the source. At depths greater than 10 mm, the absorption at the two laterally displaced positions are equivalent and slightly less than that at the mid line, suggesting that the fetal head is not being interrogated. Evaluation of the NIR measurements from the maternal abdomen in Figure 10(a) indicates that they are very similar to that observed from the tissue phantom.

Specifically, the absorption at both the lateral left and right is decreased relative to that at the mid line except at a fetal head depth of 18 mm where the absorption is increased at the lateral left and decreased at the lateral right, relative to that at the mid line. These results are congruent with that observed in Figure 7(a).

Evaluation of the NIR measurement from the tissue phantom in Figure 10(b) indicates that at a source-detector separation of 10 cm and a fetal head depth of 10 mm, the absorption is increased relative to that at the mid line when the fetal head is directly below the detector or directly below the source, although the latter case displays the maximal absorption. At fetal head depths of 20 and 30 mm, the absorption is maximal when the fetal head is directly below the source and minimal when it is directly below the detector. This suggests that the optical probe is maximally sensitive to the fetal head, when it is placed on the maternal abdomen such that the fetal head is directly above the source. At a depth of 40 mm, the absorption is equivalent and less than that at the mid line, when the fetal head is directly below the source or the detector suggesting that at this depth, the fetal head is not being interrogated. The NIR measurements from the maternal abdomen in Figure 10(b) indicates a striking similarity. Specifically, the absorption at the lateral left and right are displaced in opposite directions relative to that at the mid line, expect at a fetal head depth of 35 mm, where they are both decreased relative to that at the mid line. These results are again congruent with that observed in Figure 7(b). Figure 10 suggests that: (1) when the fetal head depth is greater than the penetration depth of light, the absorption at both the lateral left and right is decreased relative to that at the mid line, whereas (2) when the fetal head is localized, the absorption at both the lateral left and right is (a) increased relative to that at the mid line (shallow fetal head depths) or (b) unequal, with one being less than at the mid line and the other higher than that at the mid line (moderate fetal head depths).

The lack of symmetry in the NIR measurements for the case in which the fetal head is below the detector versus below the source may be attributed to the different areas of the source and detector used in these studies. Specifically, if the source and detector have the same area, there should be reciprocity when the source and detector positions are switched with each other. However, if the source and detector areas differ, reciprocity fails and switching the source and detector positions with each other, affects the NIR measurement. The companion manuscript illustrates this point through numerical and experimental investigation of the tissue phantoms, with the source-detector configurations reported here.[16]

4 Conclusions

Near infrared measurements were made from the maternal abdomen (clinical studies) and laboratory tissue phantoms (experimental studies) to gain insight into photon migration through the fetal head *in utero*. Evaluation of the results indicates the following findings. First, the fetal head is more absorbing than the maternal tissue layer. Second, there appears to be minimal intervening amniotic fluid between the maternal tissue and fetal head in the photon migration path, in the case of the late gestational fetal head *in utero*. Furthermore, the optical probe is maximally sensitive to the presence of the fetal head, when it is placed on the maternal abdomen, such that the fetal head is located directly below the light source. Finally, the optical probe is sensitive to the presence of the fetal head up to a depth of 3 cm, which is at the upper limit of fetal head depths observed in near-term patients.

These results set the precedent for several important experimental and theoretical studies that have to be conducted before fully realizing the diagnostic potential of ante-partum, transabdominal, NIR spectroscopy. First, it is necessary to develop experimental and theoretical models to measure and quantify the overlap between the photon migration path and the fetal head *in utero*. Second, it is important to relate this overlap to the accuracy and sensitivity of transabdominal, NIR spectroscopy for measuring and quantifying fetal cerebral blood oxygenation *in utero*. The development of experimental and theoretical models to quantify photon migration through the fetal head *in utero* is addressed in a companion manuscript,[16] the contents of which are briefly summarized below.

In the companion manuscript,[16] experimental and theoretical models were developed and evaluated to quantify NIR photon migration through the fetal head *in utero* for various source-detector separations, fetal head positions/depths, and fetal head optical properties. First, the previously developed cw spectrometer (Figure 1) was employed to make NIR measurements on the laboratory tissue phantoms (Figure 2), which had a fixed set of optical properties and a fixed physical geometry. Next, the NIR measurements on the laboratory tissue phantoms were compared to numerical, finite-difference simulations that provide solutions to the diffusion as well as the transport equation. This comparison was made to determine which numerical model best describes photon migration through the tissue phantom. Finally, the optimal numerical model was employed to quantify photon migration through the fetal head *in utero* for various source-detector separations, fetal head positions/depths, and fetal head optical properties. Evaluation of the results obtained indicates that these experimental and theoretical models are useful for assessing the accuracy and sensitivity of transabdominal, NIR spectroscopy for measuring and quantifying fetal cerebral blood saturation *in utero*.

Acknowledgment

This research project was funded by the National Institutes of Health (Grant No. 1R43HL61057-06) and in part by the City of New York Council Speaker's Fund for Biomedical Research: Toward the Science of Patient Care, and the Dean's Office of the College of Medicine at the State University of New York-Downstate Medical Center.

References

1. M. M. Adams, ''The continuing challenge of pre-term delivery,'' *J. Am. Med. Assoc.* **273**(2), 739–740 (1995).
2. K. B. Nelson and J. H. Ellenberg, ''Antecedents of cerebral palsy: Multivariate analysis of risk,'' *New. Engl. J. Med.* **315**, 81–86 (1986).
3. C. P. Torfs, B. van den Berg, F. W. Oechsli, and S. Cummins, ''Prenatal and perinatal factors in the etiology of cerebral palsy (see comments),'' *J. Pediatr. (St. Louis)* **116**, 615–619 (1990).
4. E. P. Schneider, J. M. Hutson, and R. H. Petrie, ''An assessment of the first decade's experience with ante-partum fetal heart rate testing,'' *Am. J. Perinatol* **5**, 134 (1988).
5. M. Helfand, and M. J. Zimmer-Gembeck, ''Practice variation and the

risk of low birth weight in a public prenatal care program,'' *Medical Care* **35**(1), 16–31 (1997).
6. J. Lavery, ''Nonstress fetal heart rate testing,'' *Clin. Obstet. Gynecol.* **25**, 689 (1982).
7. F. A. Manning, C. R. Harman, and I. Morrison, ''Fetal assessment based on fetal biophysical profile scoring,'' *Am. J. Obstet. Gynecol.* **162**, 3 (1990).
8. B. Chance et al., ''Time-resolved spectroscopy of hemoglobin and myoglobin in resting and ischemic muscle,'' *Anal. Biochem.* **174**, 698–707 (1988).
9. S. Feng, F. Zeng, and B. Chance, ''Photon migration in the presence of a single defect. A perturbation analysis,'' *Appl. Opt.* **34**(19), 3826–3837 (1995).
10. *Photon Migration Through Tissues*, B. Chance, Ed., Plenum Press, New York (1996).
11. N. Ramanujam, H. Long, M. Rode, I. Forouzan, M. Morgan, and B. Chance, ''Ante-partum transabdominal near infrared spectroscopy: feasibility of measuring photon migration through the fetal head *in utero*,'' *J. Matern Fetal Med.* **8**, 275–288 (1999).
12. M. S. Patterson, J. D. Moulton, B. C. Wilson, K. W. Berndt, and J. R. Lakowicz, ''Frequency domain reflectance for the determination of the scattering and absorption properties of tissue,'' *Appl. Opt.* **30**(31), 4474–4476 (1991).
13. V. Ntziachristos, X. H. Ma, A. G. Yodh, and B. Chance, ''Multichannel photon counting instrument for spatially resolved near infrared spectroscopy,'' *Rev. Sci. Instrum.* **70**(1), 193–201 (1999).
14. A. Duncan, J. H. Meek, M. Clemence, C. E. Elwell, L. Tyszczuk, M. Cope, and D. T. Delpy, ''Optical pathlength measurements on adult head, calf and forearm and the head of the newborn infant, using phase resolved optical spectroscopy,'' *Phys. Med. Biol.* **40**(2), 295–304 (1995).
15. *Biological Spectroscopy*, I. D. Campbell and R. A. Dwek, Eds., Benjamin/Cummings Publishing Co., Menlo Park (1984).
16. G. Vishnoi, A. H. Hielscher, N. Ramanujam, and B. Chance, ''Photon migration through the fetal head *in utero* using continuous wave, near infrared spectroscopy: development and evaluation of experimental and numerical models,'' in this issue.